Accurate UWB Radar Imaging Algorithm Using Curvilinear Scanning of Antenna

Yoriaki Abe Shouhei Kidera Tetsuo Kirimoto

Graduate School of Informatics and Engineering, University of Electro-Communications, Tokyo, Japan, abe@secure.ee.uec.ac.jp

Abstract: UWB (Ultra-wideband) pulse radars are promising as the imaging sensor for rescue robot in the near field because they have an advantage in environmental measuring. We have already proposed accurate and fast imaging algorithm as RPM (Range Points Migration), which includes estimation of the direction of arrival (DOA). However, when the algorithm assumes a curvilinear scan trajectory and an omni-directional imaging, some false images often appear due to uncertainty for the DOA estimation. To suppress false images, this paper introduces a post-processing algorithm, which limits the searching range for the DOA estimation by using the initial image. The results in numerical simulations including noisy situations show that the proposed method accomplishes accurate target imaging at the order of 1/100 wavelength, even in curvilinear scan trajectory.

Key words: UWB pulse radars, Range points migration, DOA estimation, curvilinear scan trajectory, multiple targets.

1 Introduction

UWB (Ultra-wideband) pulse radars have an advantage in environmental measuring even in critical situations such as disaster sites, where an optical measurement is hardly applied. They also have a high potential for a high-range resolution imaging, and are promising as the imaging sensor for rescue robot in the near field.

In recent years, various kinds of imaging algorithm have been proposed. Although Synthetic aperture radar (SAR) [1] is one of the most stable imaging techniques, its computational burden is so large that it is hardly applicable to real-time applications. On the other hand, the high-speed imaging algorithm called SEABED (Shape Estimation of Directly scattered waves) achieves direct and nonparametric imaging based on reversible transforms between time delay and target boundary [2], [3]. However, SEABED utilizes the derivative operations of the received data, and it enhances fluctuation of small range errors. Contrarily, Envelope realizes robust and fast imaging by utilizing the relationship between the target boundary and an envelope of circles determined by antenna locations and observed ranges [4], [5]. Although this method realizes stable imaging for simple shape targets without derivative operation, the image obtained with Envelope becomes inaccurate in the case of the target with complex boundaries. This is because it requires an appropriate range connection, which is often difficult in the case of richly interfered situations. We have already proposed accurate and fast imaging algorithm as RPM (Range Points Migration), which uses observed range points and their amplitudes to estimate the direction of arrival (DOA) [6]. Since this method is based on direct group mapping from observed ranges to target points, it requires no range connection and substantially resolves the inaccuracy for estimating complex target shapes. Although this algorithm assumes the linear scanning and confines the imaging area, it is impractical assumption especially for the application of moving robot.

First, this paper shows that when RPM does not confine the imaging area, some false images appear due to uncertainty for the DOA estimation. To resolve this difficulty, then a false image reduction algorithm is proposed, which limits the searching range for the DOA estimation using the initial RPM image. The scheme of this DOA limitation is induced by the characteristic that false images are randomly distributed regardless of the changes of the antenna position. The results in numerical simulations including noisy situations show that the proposed method successfully suppresses the false images and accomplishes accurate target imaging at the order of 1/100 wavelength, even in curvilinear scan trajectory.

2 System model

Fig. 1 shows the system model. We assume two targets with clear boundaries, one target has an asteroidal boundary and is expressed as $(x-2.5)^{\frac{2}{3}}+(z-2.5)^{\frac{2}{3}}=1$, and the other target has a circular boundary and is expressed as $(x-6.25)^2+(z-2.5)^2=0.5^2$. The conductivity and relative permittivity of the targets are set to 1.0×10^6 S/m and 1.0, respectively. We assumes that the propagation speed of the radio wave is known and constant. We also assumes

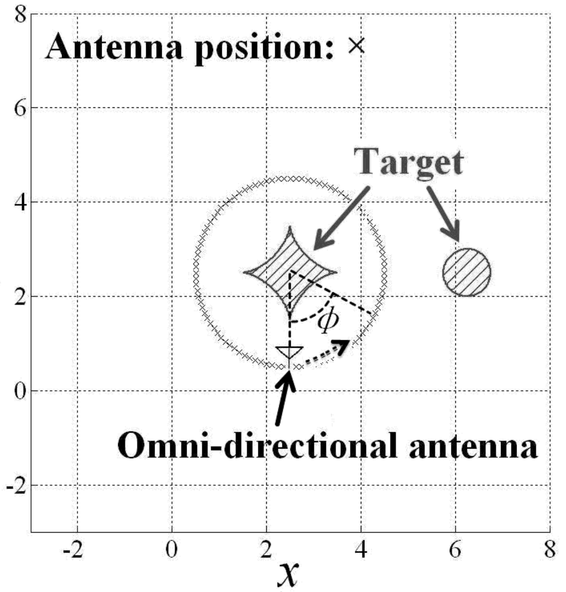

Fig 1: System model.

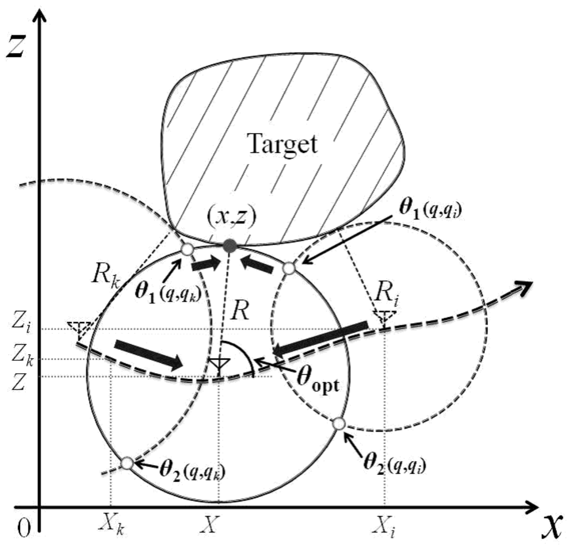

Fig 2: Relationship between the target boundary and the intersection points of the circles.

a mono-static radar. We use a mono-cycle pulse as the transmitting signal. The space where the targets and antenna are located is expressed as (x, z). The parameters are normalized by λ, which is the central wavelength of the pulse. An omni-directional antenna is scanned along the circle whose center is $(x, z) = (2.5, 2.5)$ and radius is 2λ. Any kind of curvilinear scan trajectories, even if it is not differentiable, can be principally used instead. $s'(X, Z, t)$ is defined as the electric field received at antenna location $(x, z) = (X, Z)$ at time t. $s(X, Z, t)$ is output of the Wiener filter where the detailed procedure is described in [6]. $s(X, Z, t)$ is converted to $s(X, Z, R')$ using the valuable conversion $R' = \mathrm{c}_0 t/2\lambda$ where c_0 is the speed of the radio wave. (X, Z, R) is defined as range point which is extracted from the local peaks of $s(X, Z, R')$ as

$$\frac{\partial s(X, Z, R')}{\partial R'} = 0,$$
$$s(X, Z, R') \geq \alpha \max s(X, Z, R'). \qquad (1)$$

The parameter $\alpha > 0$ is empirically determined.

3 RPM Algorithm

RPM algorithm is based on the simple principle that a target boundary point should exist on a circle, with a center at the antenna position and radius of R. Thus, each point (x, z) can be calculated using the corresponding angle of arrival, defined as DOA. Although this algorithm basically assumes the linear scanning of the antenna, it can be readily applied to curvilinear scan trajectories and realizes omni-directional imaging by calculating the intersection points of whole circles. For the DOA estimation, following function $f_k(\theta, \boldsymbol{q}, \boldsymbol{q_i})$ is introduced:

$$f_k(\theta, \boldsymbol{q}, \boldsymbol{q_i}) = \exp\left[-\frac{\{\theta - \theta_k(\boldsymbol{q}, \boldsymbol{q_i})\}^2}{2\sigma_\theta^2}\right], (k = 1, 2), \quad (2)$$

where $\boldsymbol{q} = (X, Z, R)$, $\boldsymbol{q_i} = (X_i, Z_i, R_i)$ are defined and the constant σ_θ is empirically determined. $\theta_k(\boldsymbol{q}, \boldsymbol{q_i})$ denotes the angle from the x axis to the intersection points of the circles, with parameters (X, Z, R) and (X_i, Z_i, R_i). We discriminate the two intersection points of each pair of the circles by the index k. Fig. 2 shows the relationship between the intersection points of the circles and the angle of arrival. The evaluation values $F_k(\theta; \boldsymbol{q})$ for the angle estimation is introduced as,

$$F_k(\theta; \boldsymbol{q}) = \sum_{i=1}^{N_\mathrm{q}} s(X_i, Z_i, R_i) f_k(\theta, \boldsymbol{q}, \boldsymbol{q_i})$$
$$\times \exp\left[-\frac{(X - X_i)^2 + (Z - Z_i)^2}{2\sigma_X^2}\right], (k = 1, 2), \quad (3)$$

where N_q is the total number of the range points and the constant σ_X is empirically determined. As the antenna position (X_i, Z_i) moves to (X, Z), intersection points converge to the angle of arrival and Eq. (3) have its peak near the true DOA. The optimum DOA for each $\boldsymbol{q_i}$ is calculated as,

$$\theta_{\mathrm{opt}} = \arg\max_{\theta \in \Theta} \{F_1(\theta; \boldsymbol{q}) + F_2(\theta; \boldsymbol{q})\}, \quad (4)$$

where $\Theta = \{\theta \,|\, 0 \leq \theta < 2\pi\}$. The target boundary (x, z) for each range point (X, Z, R) is expressed as,

$$\left.\begin{array}{l} x = X + R\cos\theta_{\mathrm{opt}} \\ z = Z + R\sin\theta_{\mathrm{opt}} \end{array}\right\}. \quad (5)$$

By calculating all intersection points of the circles, this extended RPM algorithm can be applied to

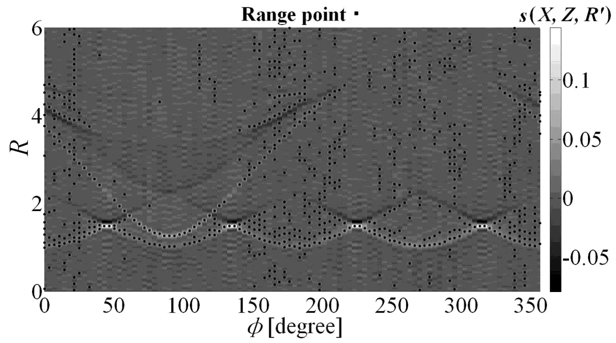

Fig 3: Output of the Wiener filter and the extracted range points for S/N = 20 dB.

curvilinear scan trajectories and does not require the confine of the imaging area. However, either of the two intersection points of the circles does not correspond to the true angle of arrival and then causes false images.

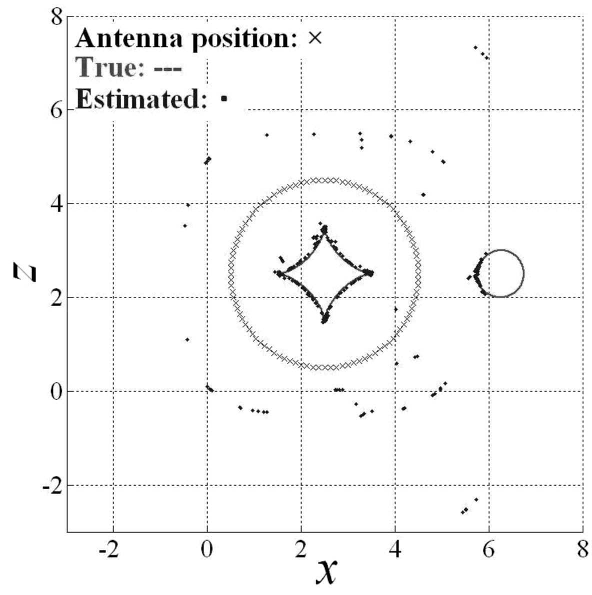

Fig 4: Estimated image with RPM algorithm for S/N = 20 dB.

4 Proposed Method Algorithm

To resolve the above problem, this paper proposes a post-processing algorithm, which limits the searching range for the DOA estimation. The motivation of the limitation is arisen from the fact that the false images are randomly distributed regardless of the changes of the antenna position. For the searching range limitation, the following function $g(\theta_l, X, Z)$ is introduced:

$$g(\theta_l, X, Z) = \exp\left[-\frac{(\theta-\theta_l)^2}{2\sigma_g^2}\right], (l = 1, ..., N_{\mathrm{T}}), \quad (6)$$

where N_{T} is the total number of the estimate target points, which is obtained by the RPM. The constant σ_g is empirically determined and θ_l denotes the angle from the x axis to the point $(x_l - X, z_l - Z)$. The evaluation value $G(\theta, X, Z)$ for the searching range at the antenna position (X, Z) is introduced as,

$$G(\theta, X, Z) = \sum_{l=1}^{N_{\mathrm{T}}} g(\theta_l, X, Z). \quad (7)$$

Eq. (7) has large values at the angle where sufficient numbers of estimated points exist. The searching range for the DOA at (X, Z) is defined as,

$$\Theta_{(X,Z)} = \{\theta \mid G(\theta, X, Z) \geq \gamma \max_{\theta} G(\theta, X, Z)\}, \quad (8)$$

where the constant γ is empirically determined. To suppress false images, we recalculate θ_{opt} for each range point (X, Z, R) using the searching range of $\Theta_{(X,Z)}$,

$$\theta_{\mathrm{opt}} = \arg\max_{\theta \in \Theta_{(X,Z)}} \{F_1(\theta; \boldsymbol{q}) + F_2(\theta; \boldsymbol{q})\}. \quad (9)$$

The procedure of the proposed method is as follows:

Step 1). Obtain θ_{opt} in Eq. (4) for all range points.
Step 2). Calculate the searching range $\Theta_{(X,Z)}$ in Eq. (8) for each antenna position.
Step 3). Recalculate θ_{opt} using Eq. (9).
Step 4). Calculate the points on the target boundary using Eq. (5).
Step 5). Remove the estimated points that satisfy,

$$\sqrt{(X_i - x)^2 + (Z_i - z)^2} \leq \kappa \min_{j} R_{i,j} \quad (10)$$

where $\kappa \leq 1$ and $R_{i,j}$ denotes the jth of the range points which are observed at (X_i, Z_i).

Step 5) suppresses false images caused by random noises because there should be no target points inside the circle, whose center is the antenna position and radius is the shortest observed range at the position. It should be noted that the proposed method does not only reduce false images but also increase the number of the accurate target points by recalculating the DOA.

5 Numerical Simulations

This section evaluates performances of RPM algorithm and the proposed method. FDTD (Finite Difference Time Domain) method is used for the calculation of received signals. Gaussian noises are added to received signals and S/N = 20 dB in this case. Here, S/N is defined as the ratio of peak instantaneous signal power to the averaged noise power after applying the matched filter. Fig. 3 shows the output of the Wiener filter and the extracted range points (X, Z, R), where ϕ denotes the angle as shown in Fig. 1. Fig. 4 shows the image estimated by RPM algorithm. $\sigma_\theta = \pi/25$, $\sigma_X = 0.5\lambda$, $\alpha = 0.3$ and $\beta = 0.2$

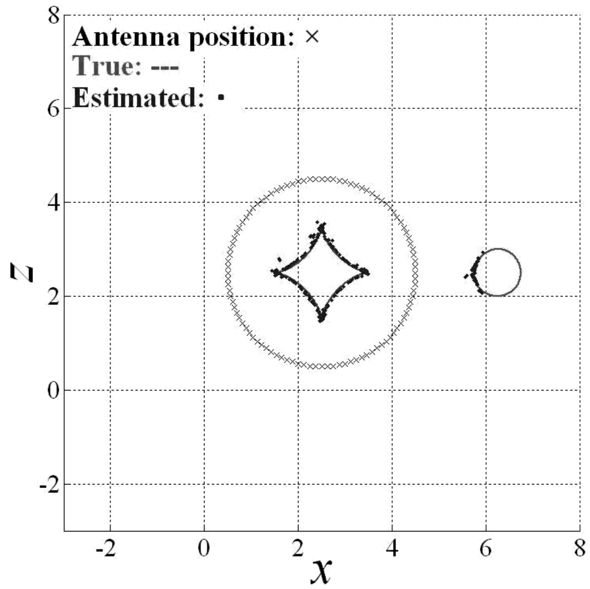

Fig 5: Estimated image with the proposed algorithm for S/N = 20 dB.

are set. This result indicates that although RPM algorithm realizes the target boundaries estimation using curvilinear scan trajectory, there are some false images outside the circular scan trajectory. These false images appear when the intersection points of the circles converge to the opposite side of the actual target. Fig. 5 shows the image estimated by the proposed algorithm. $\sigma_g = \pi/10$, $\gamma = 0.3$ and $\kappa = 0.8$ are set. It is obvious from the result that applying the post-processing algorithm significantly suppresses the false images and increase the number of target points close to the actual boundary. For a quantitative evaluation of the accuracy, $\epsilon(\boldsymbol{x}_e^i)$ is introduced as,

$$\epsilon(\boldsymbol{x}_e^i) = \min||\boldsymbol{x} - \boldsymbol{x}_e^i||, \quad (i = 1, 2, ..., N_{\mathrm{T}}), \tag{11}$$

where $\boldsymbol{x}$ and $\boldsymbol{x}_e^i$ express the location of the true target point and that of the estimated point, respectively. N_{T} is the total number of $\boldsymbol{x}_e^i$. Fig. 6 plots the number of estimated points for each value of ϵ. The value of N_{T} for each result is 303 for RPM algorithm and 270 for the proposed algorithm, respectively. The figure reveals that the number of estimated points with $\epsilon \geq 1.0\lambda$ for RPM algorithm is significantly larger than that for the proposed algorithm. Furthermore, the number of estimated points with $\epsilon \leq 0.1\lambda$ for the proposed method increases. This result shows a noticeable point that the proposed method does not only remove the false image points but also increases the points around the actual boundary using DOA recalculation. The mean values of ϵ for each result are about 0.55λ for RPM algorithm and about 0.029λ for the proposed algorithm, respectively.

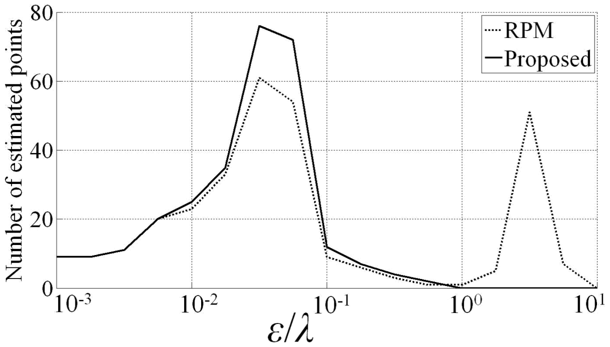

Fig 6: Error distribution for RPM algorithm and the proposed algorithm.

6 Conclusion

In this paper, we first showed that false images appear due to uncertainty for the DOA estimation in the conventional RPM algorithm when it is applied to curvilinear scan trajectories and omni-directional imaging. To suppress false images, we introduced a post-processing algorithm, which limits the searching range for the DOA estimation. The results in numerical simulations including noisy situations show that the proposed method accomplishes accurate target imaging at the order of 1/100 wavelength, even in curvilinear scan trajectory.

References

[1] D. L. Mensa, G. Heidbreder and G. Wade, Aperture Synthesis by Object Rotation in Coherent Imaging, *IEEE Trans. Nuclear Science.*, vol. 27, no. 2, pp. 989–998, Apr., 1980.

[2] T. Sakamoto and T. Sato, A target shape estimation algorithm for pulse radar systems based on boundary scattering transform, *IEICE Trans. Commun.*, vol. E87-B, no. 5, pp. 1357–1365, 2004.

[3] T. Sakamoto, A fast algorithm for 3-dimensional imaging with UWB pulse radar systems, *IEICE Trans. Commun.*, vol. E90-B, no. 3, pp. 636–644, 2007.

[4] S. Kidera, T. Sakamoto and T. Sato, A Robust and Fast Imaging Algorithm with an Envelope of Circles for UWB Pulse Radars, *IEICE Trans. Commun.*, vol. E90-B, no. 7, pp. 1801–1809, July, 2007.

[5] S. Kidera, T. Sakamoto and T. Sato, High-Resolution and Real-time UWB Radar Imaging Algorithm with Direct Waveform Compensations, *IEEE Trans. Geosci. Remote Sens.*, vol. 46, no. 11, pp. 3503–3513, Nov., 2008.

[6] S. Kidera, T. Sakamoto, T. Sato, Accurate UWB Radar 3-D Imaging Algorithm for Complex Boundary without Range Points Connections, *IEEE Trans. Geosci. Remote Sens.*, vol.48, no. 4, pp. 1993–2004, Apr., 2010.